OPTICA

Dielectric super-absorbing metasurfaces via PT symmetry breaking

Jianbo Yu,[1] Binze Ma,[1] Ao Ouyang,[1] Pintu Ghosh,[1] Hao Luo,[1] Arnab Pattanayak,[1] Sandeep Kaur,[1] Min Qiu,[2,3] Pavel Belov,[4] and Qiang Li[1,*]

[1]State Key Laboratory of Modern Optical Instrumentation, College of Optical Science and Engineering, Zhejiang University, Hangzhou 310024, China
[2]Key Laboratory of 3D Micro/Nano Fabrication and Characterization of Zhejiang Province, School of Engineering, Westlake University, Hangzhou 310024, China
[3]Institute of Advanced Technology, Westlake Institute for Advanced Study, Hangzhou 310024, China
[4]Department of Physics and Engineering, ITMO University, Russia
*Corresponding author: qiangli@zju.edu.cn

Received 6 May 2021; revised 16 August 2021; accepted 11 September 2021 (Doc. ID 430893); published 1 October 2021

Dielectric super-absorbing (>50%) metasurfaces, born of necessity to break the 50% absorption limit of an ultrathin film, offer an efficient way to manipulate light. However, in previous works, super absorption in dielectric systems was predominately realized via making two modes reach the degenerate critical coupling condition, which restricted the two modes to be orthogonal. Here, we demonstrate that in nonorthogonal-mode systems, which represent a broader range of metasurfaces, super absorption can be achieved by breaking parity-time (PT) symmetry. As a proof of concept, super absorption (100% in simulation and 71% in experiment) at near-infrared frequencies is achieved in a Si-Ge-Si metasurface with two nonorthogonal modes. Engineering PT symmetry enriches the field of non-Hermitian flat photonics, opening-up new possibilities in optical sensing, thermal emission, photovoltaic, and photodetecting devices. © 2021 Optical Society of America under the terms of the OSA Open Access Publishing Agreement

https://doi.org/10.1364/OPTICA.430893

1. INTRODUCTION

Dielectric super-absorbing (>50%) metasurfaces have attracted growing attention in that they break the 50% absorption limit of a subwavelength thickness film [1], and exhibit advantages over metallic metasurfaces, such as low Ohmic dissipation, out-of-band transparency, and CMOS compatibility [2–9]. Losses in these metasurfaces enable them to exchange energy with the surrounding environment and exhibit complex eigenvalues, making them non-Hermitian [10–13]. Originating from quantum mechanics [14], non-Hermitian physics has been used to study the characteristics of optical systems, which led to the emergence of numerous novel phenomena and applications, such as loss-induced optical non-reciprocity [15], loss-induced optical transparency [16], selective thermal emitters [17,18], unidirectional invisibility [19,20], and exceptional points (EPs)-based sensing [21–23]. Parity-time (PT) symmetric systems is a particular family of non-Hermitian systems, which are invariant under the combined action of the P ($i \to i$, $\hat{x} \to -\hat{x}$, $\hat{p} \to -\hat{p}$) and T ($i \to -i$, $\hat{x} \to \hat{x}$, $\hat{p} \to -\hat{p}$) operators. The eigenfrequencies of such systems have distinct behavior in the PT symmetry and PT symmetry-breaking regime, and this characteristic opens up new possibilities of engineering spectral properties of photonic systems [24–27].

In dielectric non-Hermitian metasurfaces, previous efforts on realizing super absorption were making two spectrally overlapped modes reach the degenerate critical coupling condition, where the radiative and non-radiative decay rates are the same for each mode [28–41]. This method restricts the two modes to be orthogonal, i.e., the coupling between them is negligible compared to their losses. Consequently, the eigenfrequencies degenerate at the diabolic point [DP, see the green dashed line in Fig. 1(b)], where the eigenvectors are orthogonal (see Supplement 1). However, when the mode coupling is non-negligible, the strong interaction between different resonances can cause mode splitting, and the two-orthogonal-mode model is invalidated under this condition.

In this work, we demonstrate super absorption in dielectric metasurfaces by breaking PT symmetry. Our method is based on a two-nonorthogonal-mode model with EP degeneracies (both eigenvectors and complex eigenfrequencies coalesce), which can represent a broader range of optical systems. As a proof of concept, super absorption at near-infrared (NIR) frequencies is achieved in a Si-Ge-Si metasurface, with two nonorthogonal quasi bound states in the continuum (QBIC) modes. In this system, PT symmetry breaking is realized by engineering the loss difference between the two modes, and it successfully suppresses the mode splitting. Our work provides a clue for engineering light trapping in non-Hermitian flat photonics, thus having broad implications in optical sensing, photodetecting, thermal emission manipulation, and photovoltaic devices.

2. THEORETICAL MODEL

We start by considering a dual-port photonic system supporting two nonorthogonal modes M_1 and M_2 [Fig. 1(a)], whose resonant frequencies before coupling are f_1 and f_2, respectively. The two modes formed within a single resonator are connected by the near-field coupling coefficient κ. The radiative decay rate corresponding to mode j ($j = 1, 2$) can be expressed as $\gamma_{j,\mathrm{R}} = \gamma_{je} + \gamma'_{je}$, where γ_{je} and γ'_{je} are radiative decay rates of mode j to Port 1 and Port 2, respectively. The total decay rate of mode j can be given by $\gamma_j = \gamma_{j,\mathrm{NR}} + \gamma_{j,\mathrm{R}}$, where $\gamma_{j,\mathrm{NR}}$ corresponds to the non-radiative decay rate of mode j. The amplitude of incoming (outgoing) wave from Port 1 is expressed as S_{1+} (S_{1-}), whereas S_{2-} represents the amplitude of the outgoing wave from Port 2. This model can describe many dielectric systems such as dielectric meta-atoms on a transparent substrate illuminated from one side by incident light.

The far-field coupling induced by the radiation in two channels is mainly determined by the symmetric properties of the two modes. Here, we suppose that one mode decays symmetrically and the other decays anti-symmetrically into two ports, which leads to a negligible far-field coupling. Otherwise, if the two modes have the same symmetric properties, the total absorption cannot exceed 50% (see Supplement 1, Section 2). The effective Hamiltonian of the two-nonorthogonal-mode system in Fig. 1(a) is given by [42–44]

$$H = \begin{bmatrix} f_1 - i\gamma_1 & \kappa \\ \kappa & f_2 - i\gamma_2 \end{bmatrix}. \tag{1}$$

When the two resonant frequencies before coupling are the same ($f_1 = f_2 = f_0$), the eigenfrequencies can be expressed as

$$f_{\mathrm{eigen}} = f_0 - i\frac{\gamma_1 + \gamma_2}{2} \pm \frac{1}{2}\sqrt{4\kappa^2 - \Delta\gamma^2}. \tag{2}$$

The behavior of f_{eigen} is controlled by the coupling coefficient κ and the loss difference $\Delta\gamma = |\gamma_1 - \gamma_2|$. There are three cases: (1) $\kappa = \Delta\gamma/2$, which is the condition where both $\mathrm{Re}(f_{\mathrm{eigen}})$ and $\mathrm{Im}(f_{\mathrm{eigen}})$ of the two modes along with their associated eigenvectors coalesce, indicating the emergence of an EP [45]; (2) $\kappa > \Delta\gamma/2$, where, under this condition, the system is in passive PT-symmetric phase, and only $\mathrm{Im}(f_{\mathrm{eigen}})$ of the two modes coincide; and (3) $\kappa < \Delta\gamma/2$, whereby the PT-symmetric phase is broken under this condition, and only $\mathrm{Re}(f_{\mathrm{eigen}})$ of the two modes coincide. The coupling coefficient at the transition point of PT-symmetric phase is $\kappa_{\mathrm{EP}} = \Delta\gamma/2$ [see the vertical gray dashed line in Fig. 1(b)].

Lineshape and Linewidth Control—The eigenfrequencies are responsible for the lineshape features of absorption spectra. When $\kappa > \kappa_{\mathrm{EP}}$, two modes exchange energy strongly with each other, leading to the mode splitting. $\mathrm{Re}(f_{\mathrm{eigen}})$ of the two modes differ from each other, and two peaks in the absorption spectrum can be seen consequently [see PT symmetry regime in Fig. 1(b)]. When $\kappa < \kappa_{\mathrm{EP}}$, $\mathrm{Re}(f_{\mathrm{eigen}})$ of the two modes coincide and so do the two absorption peaks [see PT symmetry breaking regime in Fig. 1(b)]. Therefore, to obtain single-peak absorption spectra, we should either engineer κ or $\Delta\gamma$ to make $\kappa < \kappa_{\mathrm{EP}}$, so that the coupling-induced mode splitting can be suppressed. In PT symmetry breaking regime, the quality-factors (Q-factors) are determined by the total loss ($\gamma_1 + \gamma_2$) according to the relationship $Q \propto \omega/(\gamma_1 + \gamma_2)$, indicating that the total loss needs to be suppressed to obtain narrow band absorption spectra [see Fig. 1(b)].

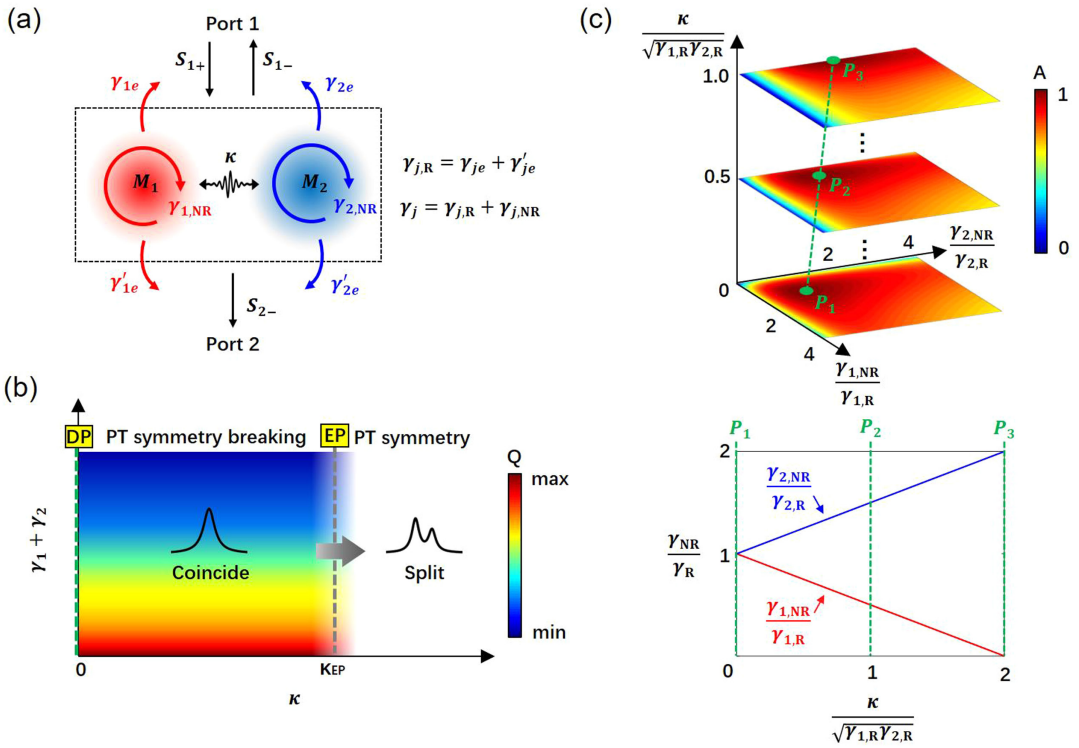

Fig. 1. (a) Diagram of a dual-port photonic system containing two nonorthogonal modes M_1 and M_2. (b) Dependence of the lineshape and Q-factors of absorption spectra on decay rates and the coupling coefficient. (c) Top: calculated absorption in the parameter space $(\gamma_{1,\mathrm{NR}}/\gamma_{1,\mathrm{R}}, \gamma_{2,\mathrm{NR}}/\gamma_{2,\mathrm{R}}, \kappa/\sqrt{\gamma_{1,\mathrm{R}}\gamma_{2,\mathrm{R}}})$, with $f_1 = f_2$. The green dots $P_{1,2,3}$ denote the unity absorption condition, and the corresponding trajectory is indicated by the green dashed line. Bottom: the value of $\gamma_{1,\mathrm{NR}}/\gamma_{1,\mathrm{R}}$ (the red solid line) and $\gamma_{2,\mathrm{NR}}/\gamma_{2,\mathrm{R}}$ (the blue solid line) under the unity absorption condition.

Amplitude Control—In PT symmetry breaking regime, the amplitudes of absorption spectra (A) can be optimized to be 100% by tuning the radiative and non-radiative decay rates. The calculated absorption in the parameter space ($\gamma_{1,\mathrm{NR}}/\gamma_{1,\mathrm{R}}$, $\gamma_{2,\mathrm{NR}}/\gamma_{2,\mathrm{R}}$, $\kappa/\sqrt{\gamma_{1,\mathrm{R}}\gamma_{2,\mathrm{R}}}$) is shown in Fig. 1(c), and unity absorption ($A = 100\%$) is achieved when both Eqs. (3) and (4) are satisfied.

$$\frac{\gamma_{1,\mathrm{NR}}}{\gamma_{1,\mathrm{R}}} = 1 - \frac{\kappa}{\sqrt{\gamma_{1,\mathrm{R}}\gamma_{2,\mathrm{R}}}}, \tag{3}$$

$$\frac{\gamma_{2,\mathrm{NR}}}{\gamma_{2,\mathrm{R}}} = 1 + \frac{\kappa}{\sqrt{\gamma_{1,\mathrm{R}}\gamma_{2,\mathrm{R}}}}. \tag{4}$$

Here, we suppose M_1 decays symmetrically, and M_2 decays anti-symmetrically. The other case is that M_1 decays anti-symmetrically, and M_2 decays symmetrically, which requires $\frac{\gamma_{1,\mathrm{NR}}}{\gamma_{1,\mathrm{R}}} = 1 + \frac{\kappa}{\sqrt{\gamma_{1,\mathrm{R}}\gamma_{2,\mathrm{R}}}}$, and $\frac{\gamma_{2,\mathrm{NR}}}{\gamma_{2,\mathrm{R}}} = 1 - \frac{\kappa}{\sqrt{\gamma_{1,\mathrm{R}}\gamma_{2,\mathrm{R}}}}$ to realize unity absorption (more details are provided in Supplement 1, Section 3). At $\kappa = 0$, the two modes are orthogonal and unity absorption necessitates the radiative decay rate to be equal to the non-radiative decay rate for each mode, which is exactly the degenerate critical coupling condition studied before, see P_1 in Fig. 1(c). When the orthogonality of the two modes is perturbed by extra coupling ($\kappa \neq 0$), unity absorption can still be achieved as long as the radiative and non-radiative decay rates meet the condition described by Eqs. (3) and (4) [see P_2 and P_3 in Fig. 1(c)].

To sum up, in order to achieve super absorption for a two-nonorthogonal-mode system, we need to engineer the following three parameters: (1) lineshape: decrease the coupling coefficient κ or increase the loss difference $\Delta\gamma$ to make $\kappa < \kappa_{\mathrm{EP}}$ so that PT symmetry is broken, and thereby the mode splitting is prevented; (2) linewidth: engineer the total loss to control the linewidth, and (3) amplitude: choose two modes with different symmetric properties, and tune the radiative and non-radiative decay rates of the two modes to satisfy Eqs. (3) and (4) so that the absorption can reach 100%.

3. EXAMPLES OF SUPER ABSORPTION VIA PT SYMMETRY BREAKING

To validate the theoretical model, a dielectric metasurface with two nonorthogonal modes is established [Fig. 2(a)]. The Si elliptical cylinders with an orientation angle θ on a SiO_2 substrate support magnetic and electric QBIC (M-QBIC and E-QBIC) modes [3,46]. The mode coupling, which is comparable to the low radiative loss of QBIC modes, mainly arises from the substrate-induced interaction between electric and magnetic dipole resonances [47], and leads to the destruction of orthogonality. A thin layer of lossy Ge is inserted in the middle of lossless Si cylinders to introduce the non-radiative loss. In this Si-Ge-Si metasurface, the radiative decay rates $\gamma_{\mathrm{E-QBIC,R}}$ and $\gamma_{\mathrm{M-QBIC,R}}$ increase with the orientation angle θ, and hardly change when Ge thickness h_2 varies (see Supplement 1, Section 4). Within the cylinders, the electric field of E-QBIC mainly concentrates in the lossy Ge layer, while that of M-QBIC is mainly in the lossless Si layer [Fig. 2(b)]. Therefore, the non-radiative decay rates $\gamma_{\mathrm{E-QBIC,NR}}$ increases faster than $\gamma_{\mathrm{M-QBIC,NR}}$ when Ge thickness h_2 increases, which causes the total loss difference $\Delta\gamma$ increases with Ge thickness h_2.

The PT-symmetric phase is tuned by changing Ge thickness h_2 [Figs. 2(c) and 2(d)]. To guarantee either $\mathrm{Re}(f_{\mathrm{eigen}})$ or $\mathrm{Im}(f_{\mathrm{eigen}})$ of the two modes coinciding at different h_2, P_x is varied from 0.712 μm to 0.733 μm in the calculation (see Table 1 in Supplement 1, Section 4). At $h_2 < 0.038$ μm, the total loss

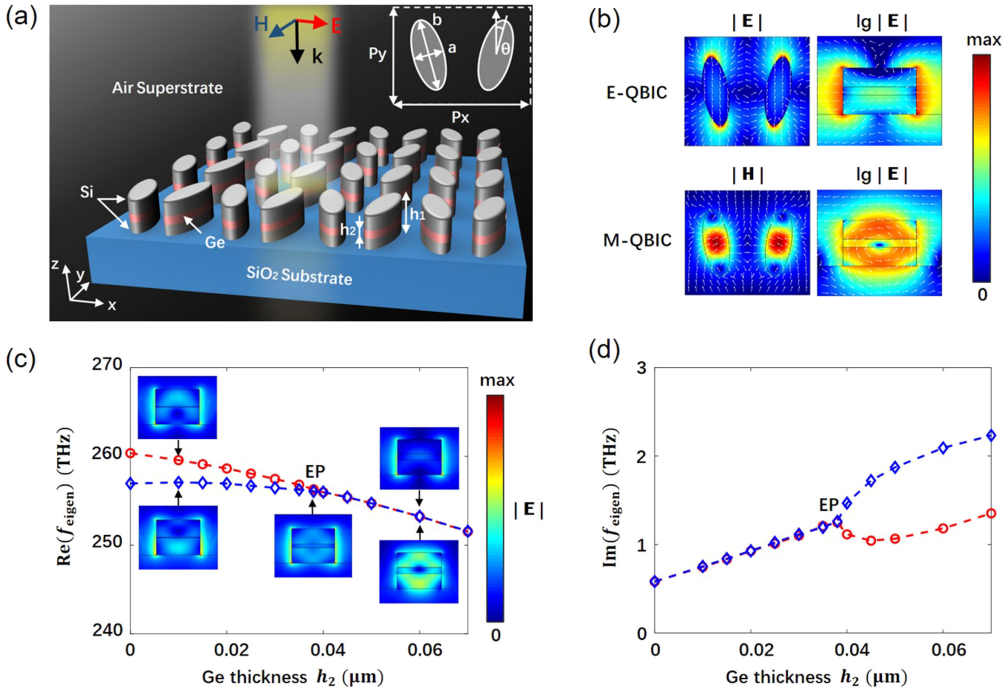

Fig. 2. (a) Schematic of the dielectric metasurface. (b) The electric and magnetic field distribution for the E-QBIC and M-QBIC, respectively. The color shows the field distribution at the plane $z = h_1/2$ (left) and $x = P_x/4$ (right). The arrows show the direction of the fields. (c) Calculated $\mathrm{Re}(f_{\mathrm{eigen}})$ of the two modes corresponding to varying Ge thickness h_2. Insets show the corresponding electric field distribution of the eigenmodes. (d) Calculated $\mathrm{Im}(f_{\mathrm{eigen}})$ of the two modes versus Ge thickness h_2. In the calculation, the following parameters are used: $h_1 = 0.330$ μm, $\theta = 9°$, $a = 0.075$ μm, $b = 0.225$ μm, $P_y = 0.740$ μm, and P_x is tuned from 0.712 μm to 0.733 μm to make either $\mathrm{Re}(f_{\mathrm{eigen}})$ or $\mathrm{Im}(f_{\mathrm{eigen}})$ of the two modes coincide at different h_2.

difference $\Delta\gamma$ is not large enough to compensate for the coupling, indicating the system is in PT-symmetric phase. The field distributions are distorted due to strong mode coupling. At $h_2 = 0.038$ μm, both Re(f_{eigen}) and Im(f_{eigen}) of the two modes coalesce at EP. The electric field distributions of the two eigenmodes are the same, since two corresponding eigenvectors are parallel at EP. At $h_2 > 0.038$μm, the system is in PT symmetry broken phase. Under this condition, Re(f_{eigen}) of the two modes coincide. The weak coupling compared with the loss difference makes the two eigenmodes have distinct field distributions. In the simulation, eigenfrequencies are calculated using the complex refractive-index of the lossy Ge, and the eigenmodes distributions can be seen in the insets of Fig. 2(c) and Supplement 1, Section 5.

The dependence of eigenfrequencies on both Ge thickness h_2 and the cylinder thickness h_1 are calculated [Figs. 3(a) and 3(b)]. At $h_2 = 0.010$μm, PT symmetry is not broken, indicating two modes have different Re(f_{eigen}) and the same Im(f_{eigen}) at the point marked with a rhombus in Fig. 3(d), which leads to an avoided crossing in the absorption spectra. Two peaks can be observed in the absorption spectra whose amplitudes are less than 0.5 [Fig. 3(e)]. At $h_2 = 0.038$ μm, both Re(f_{eigen}) and Im(f_{eigen}) of the two modes coincide at the EP [stars in Figs. 3(f) and 3(g)]. The superposition of the two modes makes the absorption peak larger than 0.5 [Fig. 3(h)]. At $h_2 = 0.050$ μm, PT symmetry is broken and two modes have the same Re(f_{eigen}) and different Im(f_{eigen}) at the point marked with a circle in Fig. 3(i). No mode splitting can be seen due to the coincidence of Re(f_{eigen}), thus the absorption spectra corresponding to the two modes also show a crossing, and super absorption is obtained [Fig. 3(k)].

The super absorption resulting from breaking PT symmetry is experimentally validated by fabricating Si-Ge-Si metasurfaces with different periods P_x. Here, Ge thickness $h_2 = 0.040$ μm corresponds to the case in which the absorption can reaches unity in simulation. The corresponding simulated eigenfrequencies and absorption spectra are plotted in Fig. 4(a) and Fig. 4(b), respectively. The PT symmetry breaking condition is marked with the gray dashed line. The measured absorption spectra of the fabricated Si-Ge-Si metasurfaces are provided in Fig. 4(c). At $P_x = 0.790$ μm, the M-QBIC and E-QBIC modes are spectrally separated. As P_x is gradually decreased, two absorption peaks cross due to the breaking of PT symmetry. When P_x is decreased further, the two peaks gradually separate again. At $P_x = 0.710$ μm,

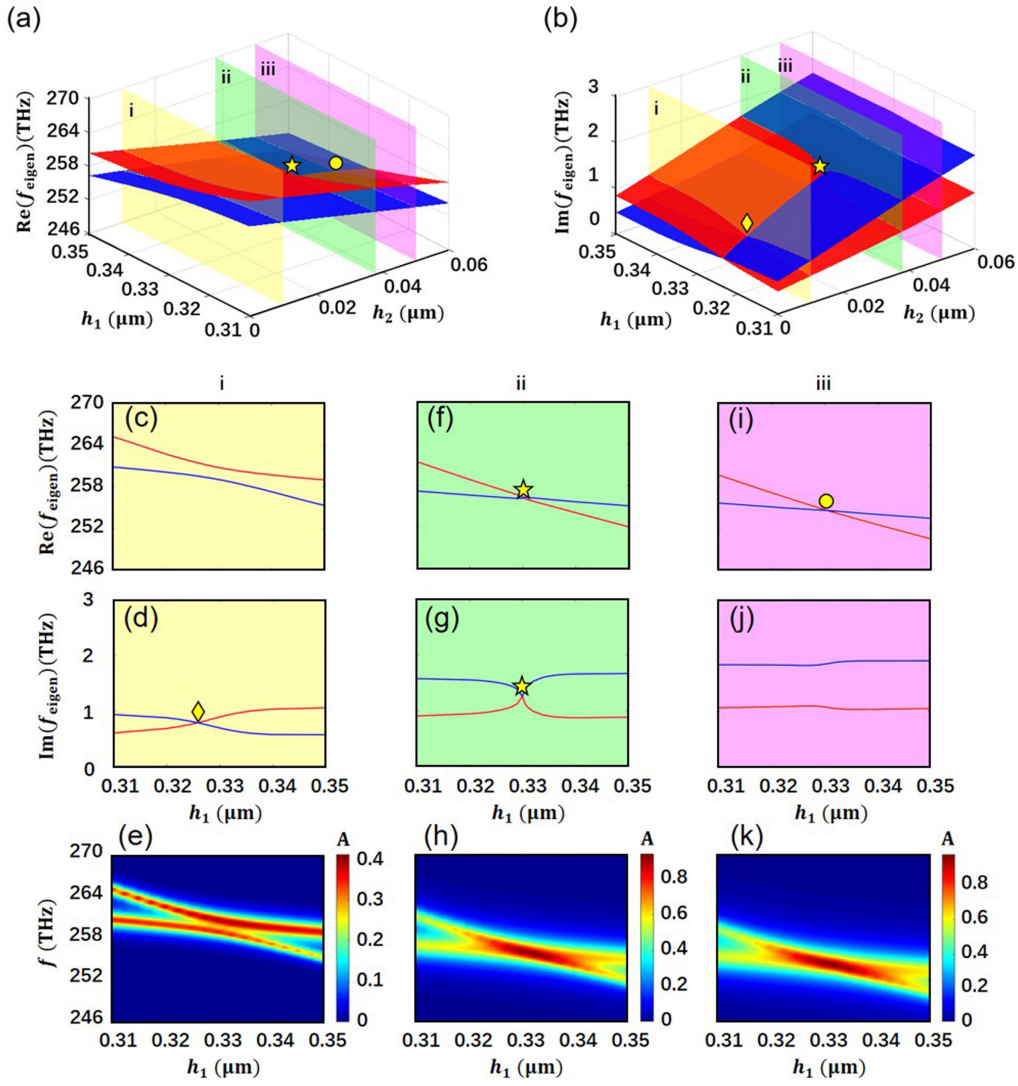

Fig. 3. Calculated (a) Re(f_{eigen}) and (b) Im(f_{eigen}) of the two modes (blue and red) in the parameter space (h_1, h_2). Re(f_{eigen}), Im(f_{eigen}), and absorption spectra at three typical h_2 values are shown: (c-e) $h_2 = 0.010$ μm, (f-h) $h_2 = 0.038$ μm, and (i-k) $h_2 = 0.050$ μm. The points marked with a rhombus (d), stars (f, g), and a circle (i) correspond to PT-symmetric phase, EP, and PT symmetry broken phase, respectively.

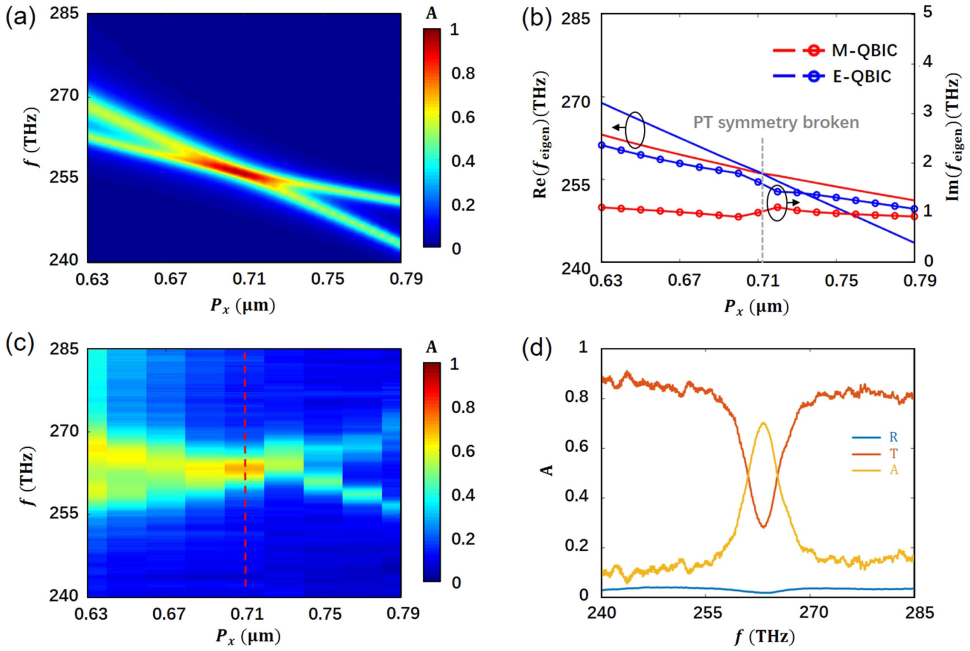

Fig. 4. (a) Simulated absorption spectra at different P_x with Ge thickness $h_2 = 0.040$ μm. The other parameters are the same as those specified above. (b) Corresponding eigenfrequencies at different P_x, the solid lines denote the real part, and the dotted lines denote the imaginary part. The vertical gray dashed line denotes PT symmetry broken phase. (c) Measured absorption spectra at different P_x with Ge thickness $h_2 = 0.040$ μm. (d) Reflection (blue), transmission (red), and absorption spectra (orange) at $P_x = 0.710$ μm, which corresponds to the red dashed line in (c).

super absorption (71%) with Q-factor ∼41 is achieved [Fig. 4(d)]. The deviation of absorption spectra in the experiment from the simulated results arises due to the fabrication imperfection, such as reduced cylinder size after etching. More details regarding the fabrication process and spectra measurement are provided in Supplement 1, Section 6.

4. CONCLUSIONS

In conclusion, we demonstrate that super absorption in dielectric metasurfaces can be achieved by breaking PT symmetry. Utilizing two coupled modes, our work provides a novel method of breaking the 50% absorption limit and achieving super absorption in dielectric metasurfaces. In previous works, dielectric super absorption was predominately realized via making two orthogonal modes reach the degenerate critical coupling condition. To guarantee the orthogonality, the losses of two modes should be large enough to preclude the influence of mode coupling, which usually makes the Q-factors low (∼ 10) [32–34,36]. Breaking PT symmetry provides an effective way to achieve super absorption in high-Q dielectric systems where the losses are comparable to the mode coupling. Besides, different from most previous experimental works where the PT-symmetric phase is broken by decreasing the coupling strength [21,48], the method of increasing the loss difference presented in this work enriches the field of PT-symmetric phase engineering. Moreover, the high-Q and out-of-band transparent properties make this dielectric absorber promising for applications in optical sensing and photodetecting devices. The working frequencies of these devices can be further extended to mid-infrared (MIR) and terahertz (THz) frequencies by replacing Si and Ge with other combination of materials: for MIR range, lossless Ge and lossy $Ge_2Sb_2Te_5$ (GST) [49,50], VO_2 [51]; and for THz range, lossless Si and lossy doped-Si [52]. Finally, we believe that the study of engineering PT-symmetric phase in low-loss dielectric systems can lead to the generation of non-Hermitian devices with novel properties, such as selective thermal emitters with high coherence, and highly sensitive spectrally tunable metasurfaces with multiple functionalities.

Funding. National Key Research and Development Program of China (2017YFA0205700); National Natural Science Foundation of China (61775194, 61950410608, 61975181).

Disclosures. The authors declare no conflicts of interest.

Data availability. Data underlying the results presented in this paper are not publicly available at this time but may be obtained from the authors upon reasonable request.

Supplemental document. See Supplement 1 for supporting content.

REFERENCES

1. S. J. Kim, J. Park, M. Esfandyarpour, E. F. Pecora, P. G. Kik, and M. L. Brongersma, "Superabsorbing, artificial metal films constructed from semiconductor nanoantennas," Nano Lett. **16**, 3801–3808 (2016).
2. E. Mikheeva, J. B. Claude, M. Salomoni, J. Wenger, J. Lumeau, R. Abdeddaim, A. Ficorella, A. Gola, G. Paternoster, M. Paganoni, E. Auffray, P. Lecoq, and S. Enoch, "CMOS-compatible all-dielectric metalens for improving pixel photodetector arrays," APL Photon. **5**, 116105 (2020).
3. A. Tittl, A. Leitis, M. Liu, F. Yesilkoy, D. Y. Choi, D. N. Neshev, Y. S. Kivshar, and H. Altug, "Imaging-based molecular barcoding with pixelated dielectric metasurfaces," Science **360**, 1105–1109 (2018).
4. K. Vynck, D. Felbacq, E. Centeno, A. I. Cabuz, D. Cassagne, and B. Guizal, "All-dielectric rod-type metamaterials at optical frequencies," Phys. Rev. Lett. **102**, 133901 (2009).
5. A. B. Evlyukhin, S. M. Novikov, U. Zywietz, R. L. Eriksen, C. Reinhardt, S. I. Bozhevolnyi, and B. N. Chichkov, "Demonstration of magnetic dipole resonances of dielectric nanospheres in the visible region," Nano Lett. **12**, 3749–3755 (2012).
6. A. I. Kuznetsov, A. E. Miroshnichenko, M. L. Brongersma, Y. S. Kivshar, and B. Luk'yanchuk, "Optically resonant dielectric nanostructures," Science **354**, aag2472 (2016).

7. J. C. Ginn, I. Brener, D. W. Peters, J. R. Wendt, J. O. Stevens, P. F. Hines, L. I. Basilio, L. K. Warne, J. F. Ihlefeld, P. G. Clem, and M. B. Sinclair, "Realizing optical magnetism from dielectric metamaterials," Phys. Rev. Lett. **108**, 097402 (2012).
8. I. Staude, A. E. Miroshnichenko, M. Decker, N. T. Fofang, S. Liu, E. Gonzales, J. Dominguez, T. S. Luk, D. N. Neshev, I. Brener, and Y. S. Kivshar, "Tailoring directional scattering through magnetic and electric resonances in subwavelength silicon nanodisks," ACS Nano **7**, 7824–7832 (2013).
9. S. Jahani and Z. Jacob, "All-dielectric metamaterials," Nat. Nanotechnol. **11**, 23–36 (2016).
10. R. El-Ganainy, K. G. Makris, M. Khajavikhan, Z. H. Musslimani, S. Rotter, and D. N. Christodoulides, "Non-Hermitian physics and PT symmetry," Nat. Phys. **14**, 11–19 (2018).
11. C. M. Bender, "Making sense of non-Hermitian Hamiltonians," Rep. Prog. Phys. **70**, 947–1018 (2007).
12. K. Kawabata, K. Shiozaki, M. Ueda, and M. Sato, "Symmetry and topology in Non-Hermitian physics," Phys. Rev. X **9**, 041015 (2019).
13. M. A. Miri and A. Alu, "Exceptional points in optics and photonics," Science **363**, eaar7709 (2019).
14. M. Bender and S. Boettcher, "Real spectra in non-Hermitian Hamiltonians having PT symmetry," Phys. Rev. Lett. **80**, 5243 (1998).
15. X. Huang, C. Lu, C. Liang, H. Tao, and Y. C. Liu, "Loss-induced nonreciprocity," Light Sci. Appl. **10**, 30 (2021).
16. A. Guo, G. J. Salamo, D. Duchesne, R. Morandotti, M. Volatier-Ravat, V. Aimez, G. A. Siviloglou, and D. N. Christodoulides, "Observation of PT-symmetry breaking in complex optical potentials," Phys. Rev. Lett. **103**, 093902 (2009).
17. C. F. Doiron and G. V. Naik, "Non-Hermitian selective thermal emitters using metal-semiconductor hybrid resonators," Adv. Mater. **31**, 1904154 (2019).
18. X. Zhang, Z. Zhang, Q. Wang, S. Zhu, and H. Liu, "Controlling thermal emission by parity-symmetric Fano resonance of optical absorbers in metasurfaces," ACS Photon. **6**, 2671–2676 (2019).
19. Z. Lin, H. Ramezani, T. Eichelkraut, T. Kottos, H. Cao, and D. N. Christodoulides, "Unidirectional invisibility induced by PT-symmetric periodic structures," Phys. Rev. Lett. **106**, 213901 (2011).
20. L. Feng, Y. L. Xu, W. S. Fegadolli, M. H. Lu, J. E. Oliveira, V. R. Almeida, Y. F. Chen, and A. Scherer, "Experimental demonstration of a unidirectional reflectionless parity-time metamaterial at optical frequencies," Nat. Mater. **12**, 108–113 (2013).
21. J. H. Park, A. Ndao, W. Cai, L. Hsu, A. Kodigala, T. Lepetit, Y. H. Lo, and B. Kanté, "Symmetry-breaking-induced plasmonic exceptional points and nanoscale sensing," Nat. Phys. **16**, 462–468 (2020).
22. W. Chen, S. K. Ozdemir, G. Zhao, J. Wiersig, and L. Yang, "Exceptional points enhance sensing in an optical microcavity," Nature **548**, 192–196 (2017).
23. H. Hodaei, A. U. Hassan, S. Wittek, H. Garcia-Gracia, R. El-Ganainy, D. N. Christodoulides, and M. Khajavikhan, "Enhanced sensitivity at higher-order exceptional points," Nature **548**, 187–191 (2017).
24. L. Chang, X. Jiang, S. Hua, C. Yang, J. Wen, L. Jiang, G. Li, G. Wang, and M. Xiao, "Parity-time symmetry and variable optical isolation in active-passive-coupled microresonators," Nat. Photonics **8**, 524–529 (2014).
25. T. Kottos, "Broken symmetry makes light work," Nat. Phys. **6**, 166–167 (2010).
26. C. E. Rüter, K. G. Makris, R. El-Ganainy, D. N. Christodoulides, M. Segev, and D. Kip, "Observation of parity-time symmetry in optics," Nat. Phys. **6**, 192–195 (2010).
27. A. Tuniz, T. Wieduwilt, and M. A. Schmidt, "Tuning the effective PT phase of plasmonic eigenmodes," Phys. Rev. Lett. **123**, 213903 (2019).
28. J. R. Piper, V. Liu, and S. Fan, "Total absorption by degenerate critical coupling," Appl. Phys. Lett. **104**, 251110 (2014).
29. T. Siday, P. P. Vabishchevich, L. Hale, C. T. Harris, T. S. Luk, J. L. Reno, I. Brener, and O. Mitrofanov, "Terahertz detection with perfectly-absorbing photoconductive metasurface," Nano Lett. **19**, 2888–2896 (2019).
30. J. Y. Suen, K. Fan, and W. J. Padilla, "A zero-rank, maximum nullity perfect electromagnetic wave absorber," Adv. Opt. Mater. **7**, 1801632 (2019).
31. K. Fan, J. Zhang, X. Liu, G. F. Zhang, R. D. Averitt, and W. J. Padilla, "Phototunable dielectric Huygens' metasurfaces," Adv. Mater. **30**, 1800278 (2018).
32. J. Tian, H. Luo, Q. Li, X. Pei, K. Du, and M. Qiu, "Near-infrared super-absorbing all-dielectric metasurface based on single-layer germanium nanostructures," Laser Photon. Rev. **12**, 1800076 (2018).
33. K. Fan, J. Y. Suen, X. Liu, and W. J. Padilla, "All-dielectric metasurface absorbers for uncooled terahertz imaging," Optica **4**, 601–604 (2017).
34. X. Ming, X. Liu, L. Sun, and W. J. Padilla, "Degenerate critical coupling in all-dielectric metasurface absorbers," Opt. Express **25**, 24658–24669 (2017).
35. J. Tian, Q. Li, P. A. Belov, R. K. Sinha, W. Qian, and M. Qiu, "High-Q all-dielectric metasurface: super and suppressed optical absorption," ACS Photon. **7**, 1436–1443 (2020).
36. C. Y. Yang, J. H. Yang, Z. Y. Yang, Z. X. Zhou, M. G. Sun, V. E. Babicheva, and K. P. Chen, "Nonradiating silicon nanoantenna metasurfaces as narrowband absorbers," ACS Photon. **5**, 2596–2601 (2018).
37. M. Yang, C. Meng, C. Fu, Y. Li, Z. Yang, and P. Sheng, "Subwavelength total acoustic absorption with degenerate resonators," Appl. Phys. Lett. **107**, 104104 (2015).
38. K. Fan, I. V. Shadrivov, A. E. Miroshnichenko, and W. J. Padilla, "Infrared all-dielectric Kerker metasurfaces," Opt. Express **29**, 10518–10526 (2021).
39. V. Romero-García, N. Jiménez, J. P. Groby, A. Merkel, V. Tournat, G. Theocharis, O. Richoux, and V. Pagneux, "Perfect absorption in mirror-symmetric acoustic metascreens," Phys. Rev. Appl. **14**, 054055 (2020).
40. L. L. Hale, P. P. Vabischevich, T. Siday, C. T. Harris, T. S. Luk, S. J. Addamane, J. L. Reno, I. Brener, and O. Mitrofanov, "Perfect absorption in GaAs metasurfaces near the bandgap edge," Opt. Express **28**, 35284–35296 (2020).
41. N. Jimenez, V. Romero-Garcia, V. Pagneux, and J. P. Groby, "Rainbow-trapping absorbers: broadband, perfect and asymmetric sound absorption by subwavelength panels for transmission problems," Sci. Rep. **7**, 13595 (2017).
42. W. Suh, Z. Wang, and S. Fan, "Temporal coupled-mode theory and the presence of non-orthogonal modes in lossless multimode cavities," IEEE J. Quantum Electron. **40**, 1511–1518 (2004).
43. X. Zhao, C. Chen, K. Kaj, I. Hammock, Y. Huang, R. D. Averitt, and X. Zhang, "Terahertz investigation of bound states in the continuum of metallic metasurfaces," Optica **7**, 1548–1554 (2020).
44. J. Lin, M. Qiu, X. Zhang, H. Guo, Q. Cai, S. Xiao, Q. He, and L. Zhou, "Tailoring the lineshapes of coupled plasmonic systems based on a theory derived from first principles," Light Sci. Appl. **9**, 158 (2020).
45. S. K. Ozdemir, S. Rotter, F. Nori, and L. Yang, "Parity-time symmetry and exceptional points in photonics," Nat. Mater. **18**, 783–798 (2019).
46. M. Liu and D. Y. Choi, "Extreme Huygens' metasurfaces based on quasi-bound states in the continuum," Nano Lett. **18**, 8062–8069 (2018).
47. A. E. Miroshnichenko, A. B. Evlyukhin, Y. S. Kivshar, and B. N. Chichkov, "Substrate-induced resonant magnetoelectric effects for dielectric nanoparticles," ACS Photon. **2**, 1423–1428 (2015).
48. F. Zhong, K. Ding, Y. Zhang, S. Zhu, C. T. Chan, and H. Liu, "Angle-resolved thermal emission spectroscopy characterization of non-Hermitian metacrystals," Phys. Rev. Appl. **13**, 014071 (2020).
49. Z. Xu, H. Luo, H. Zhu, Y. Hong, W. Shen, J. Ding, S. Kaur, P. Ghosh, M. Qiu, and Q. Li, "Nonvolatile optically reconfigurable radiative metasurface with visible tunability for anticounterfeiting," Nano Lett. **21**, 5269–5276 (2021).
50. Y. Qu, Q. Li, K. Du, L. Cai, J. Lu, and M. Qiu, "Dynamic thermal emission control based on ultrathin plasmonic metamaterials including phase-changing material GST," Laser Photon. Rev. **11**, 1700091 (2017).
51. Z. Xu, Q. Li, K. Du, S. Long, Y. Yang, X. Cao, H. Luo, H. Zhu, P. Ghosh, W. Shen, and M. Qiu, "Spatially resolved dynamically reconfigurable multilevel control of thermal emission," Laser Photon. Rev. **14**, 1900162 (2020).
52. M. van Exter and D. Grischkowsky, "Optical and electronic properties of doped silicon from 0.1 to 2 THz," Appl. Phys. Lett. **56**, 1694–1696 (1990).

202.119.42.173 (ts 2021-10-09 10:43:36)